



Published in final edited form as:

ACS Appl Bio Mater. 2020 May 18; 3(5): 2897–2909. doi:10.1021/acsabm.9b00851.

In Vitro Reconstitution of an Intestinal Mucus Layer Shows That Cations and pH Control the Pore Structure That Regulates Its Permeability and Barrier Function

Abhinav Sharma,

Department of Chemical Engineering, University of Massachusetts, Amherst, Massachusetts 01003, United States

Jun-Goo Kwak,

Department of Chemical Engineering, University of Massachusetts, Amherst, Massachusetts 01003, United States

Kristopher W. Kolewe,

Department of Chemical Engineering, University of Massachusetts, Amherst, Massachusetts 01003, United States

Jessica D. Schiffman,

Department of Chemical Engineering and Institute for Applied Life Sciences, University of Massachusetts, Amherst, Massachusetts 01003, United States

Neil S. Forbes,

Department of Chemical Engineering, Molecular and Cellular Biology Graduate Program, and Institute for Applied Life Sciences, University of Massachusetts, Amherst, Massachusetts 01003, United States

Jungwoo Lee

Department of Chemical Engineering, Molecular and Cellular Biology Graduate Program, and Institute for Applied Life Sciences, University of Massachusetts, Amherst, Massachusetts 01003, United States

* **Corresponding Authors:** Neil S. Forbes – Phone: +1 413 577 0132; forbes@umass.edu; Jungwoo Lee – Phone: +1 413 545 6290; jungwoo@umass.edu.

Author Contributions

A.S., N.S.F., and J.L. conceived the project, designed experiments, and analyzed and interpreted the results. A.S., J.-G.K., and J.L. conducted experiments. K.W.K. and J.D.S. conducted rheological characterization of reconstituted PSIM and analyzed the results. All authors participated in the writing of the manuscript.

Supporting Information

The Supporting Information is available free of charge at <https://pubs.acs.org/doi/10.1021/acsabm.9b00851>.

Supplementary figures describing DNase treatment of PSIM for reduction of contaminant DNA (Figure S1), theoretical calculation of mucus yield from porcine small intestine (Figure S2), absorbance profile of PSIM in the pH range 2–7 (Figure S3), rheological characterization of mucin extract (Figure S4), and comparison of PSIM versus commercial porcine gastric mucin (PGM) gel formation (Figure S5) (PDF)

Bacterial motility in PSIM with pH change (GFP tagged *E. coli*) (AVI)

Bacterial motility in PSIM with pH change (GFP tagged *Salmonella*) (AVI)

Reconstituted PSIM reversible bulk property changes with pH (AVI)

Ca²⁺- and EDTA-dependent reversible viscoelastic property change in PSIM (AVI)

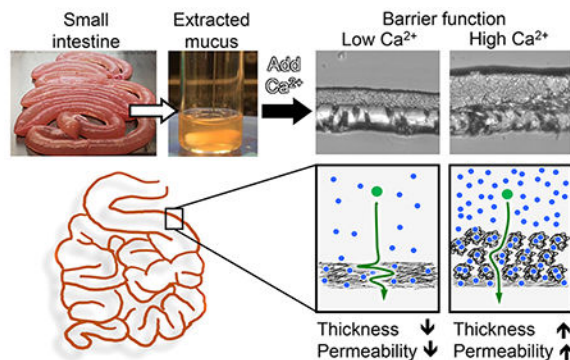
Complete contact information is available at: <https://pubs.acs.org/doi/10.1021/acsabm.9b00851>

The authors declare no competing financial interest.

Abstract

Dysfunction of the intestinal mucus barrier causes disorders such as ulcerative colitis and Crohn's disease. The function of this essential barrier may be affected by the periodically changing luminal environment. We hypothesized that the pH and ion concentration in mucus control its porosity, molecular permeability, and the penetration of microbes. To test this hypothesis, we developed a scalable method to extract porcine small intestinal mucus (PSIM). The aggregation and porosity of PSIM were determined using rheometry, spectrophotometry, and microscopy. Aggregation of PSIM at low pH increased both the elastic (G') and viscous (G'') moduli, and it slowed the transmigration of pathogenic *Salmonella*. Molecular transport was dependent on ion concentration. At moderate concentrations, many microscopic aggregates (2–5 μm in diameter) impeded diffusion. At higher concentrations, PSIM formed aggregate islands, increasing both porosity and diffusion. This in vitro model could lead to a better understanding of mucus barrier functions and improve the treatment of intestinal diseases.

Graphical Abstract



Keywords

Intestine; Mucus; Scalable extraction; Barrier function; Transport; Sol–gel transition; In vitro

INTRODUCTION

The role of mucus in the intestines is incompletely understood. The mucus layer functions as a selective biological barrier that permits the transport of digested molecules while protecting the underlying epithelial tissue.^{1–3} The content in the lumen is continually changing, and the mucus layer must respond to its environment by being a barrier to some components while being permeable to others.² The rheology and microscopic structure of mucus affects its ability to prevent bacterial infiltration.^{4,5} Many diseases involve dysfunction of the mucus barrier, such as inflammatory bowel diseases,^{6–8} cystic fibrosis,⁹ and colorectal cancer.^{10,11} In diseased states, breakdown of the mucus microstructure increases bacterial infection.^{12,13} Two factors that have been shown to affect these structural properties are the local pH and cation content.¹⁴ An experimental model that can expand the understanding of these mechanisms would be an essential tool to address diseases of the intestines.

The mesh-like structure of the mucus barrier enables it to promote nutrient absorption while acting as a barrier to infection. Mucus is primarily composed of mucin proteins. In both the large intestine and small intestine, mucus is composed predominantly of MUC2, which is one of the 21 known proteins in the MUC family.^{15,16} In the small intestine, where most nutrient absorption occurs, the mucus barrier is thin (20–100 μm thick), which facilitates molecular transport while maintaining tissue sterility against luminal microbes.^{17,18} In the large intestine, the mucus barrier is thicker (700–1000 μm), which physically shields the epithelial lining from the high density of microbiota.^{19–21} In the large intestine, the mucus layer is composed of a tightly bound inner layer and a loosely bound outer layer.²² Secreted mucus traps invading bacteria, which are eliminated with the luminal content.^{23,24}

The local environment around the mucus layer greatly affects its structural properties. The most well-studied environmental factor is pH, which has a strong effect on the rheology of mucus.^{25,26} In acidic environments, mucus is elastic and gel-like, but in neutral and basic environments, it behaves more like a liquid solution.²⁵ Mucin proteins have a bottlebrush-like structure with a protein backbone and glycan side chains²⁷ (Figure 1A). At acidic pH values, mucins change conformation and expose cysteine-rich hydrophobic regions on the protein backbone, which leads to hydrophobic interactions and gelation.^{28,29} In addition to pH, other factors may affect the structure of mucus.³⁰ Calcium ions (Ca^{2+}) play an important role in regulating intracellular mucin storage and secretion from goblet cells.^{14,31} The binding of Ca^{2+} with the glycan side chains causes dense packing of the mucin polymeric chains.^{14,32,33} In the intestines, where the luminal pH is neutral,³⁴ dietary calcium may have a greater effect on mucus structure and its barrier function. After ingesting food, the availability of calcium and other ionic molecules in the gastro-intestinal tract is increased.^{35,36} Depending on the feed state, the luminal Ca^{2+} concentration varies between 5 mM and 20 mM.^{35,37}

Much of current *in vitro* research has used mucus extracted from the stomach.^{38,39} It is plentiful, less contaminated with bacterial components, and its extraction is straightforward. This material has been instrumental in demonstrating its pH-dependent behavior and barrier function.^{26,29,40–42} Commercially available gastro-intestinal mucus is derived from porcine stomachs. A limitation of this material is that gastric mucins have a different biochemical structure from intestinal mucins. Gastric mucus is mostly MUC5AC and MUC6,⁴³ whereas the intestines are primarily MUC2.¹⁵ In addition, commercial mucin has poor gel-forming capability.⁴⁴ This transition is an essential aspect of the primary barrier function of mucus.

In the absence of a commercial source, there are two predominant methods used to study intestinal mucus derived from rodent, large animal, or human tissues. The most common is the direct scraping of mucus from the intestinal wall. Scraped mucus has been used to demonstrate that large nanoparticles, if properly coated, can rapidly penetrate mucus, compared to smaller nanoparticles.⁴⁵ It has also been shown that the interaction of mucus with food-associated stimuli such as lipids, calcium, and pH, significantly reduce the transport of microspheres.³⁵ An important limitation of this scraping technique is that contamination of unprocessed mucus with cellular debris can cause unwanted immunological responses or cytotoxicity *in vitro*.⁴⁶ Alternatively, several studies have purified the mucin proteins from intestinal mucus.^{47,48} Purified mucins retain the

rheological properties of mucus^{49,50} and have been used to show that mucin chain entanglement is dominant at neutral pH and high concentration.⁵¹ At low pH, the gel formation is accompanied by the formation of large-scale heterogeneities within the mucin solutions.⁵² This purification method has limited yield, is time-intensive, and requires costly specialized equipment, which limits its widespread use for effective recapitulation of mucus barriers with physiological thickness and concentration in vitro. In recent years, little progress has been made in advancing mucus extraction protocols on a large scale.^{50,53,54}

The goal of our study was to develop a method for extracting intestinal mucus and to quantify the effect of environmental factors on its barrier properties. We hypothesized that the permeability and barrier function of intestinal mucus is reversible and changes in response to the Ca²⁺ ions in the local environment. To quantify these properties, the extraction method must be able to produce sufficient quantities of mucus that retained its pH-responsive rheology and contained minimal cellular contaminants. A systematic process was used to determine the extraction conditions that would result in a high yield, cause minimal cellular damage, and isolate mucus that would form a gel. Spectrometric and rheometric measurements were used to quantify the absorbance and physical properties, in response to acidic and high calcium environments. The physical structure of mucus proteins in these environments was determined by microscopy. The ability of mucus to limit molecular diffusion and bacterial penetration was determined in an in vitro mucus barrier model. This development of a high-throughput extraction method will enhance mucus research. Understanding the mechanisms that control the barrier function of mucus will ultimately lead to better treatments of mucus-related diseases of the intestines.

RESULTS

Extraction of Natural Mucus.

We have developed a new method to extract mucus from porcine small intestines (Figure 1B). The goal of the design process was to develop a method that isolates mucus while retaining its pH-responsive rheology and minimizing the inclusion of cellular contaminants. This method was based on the observation that, after mucus is scraped from the intestine, it dissolves in an alkaline solution. To determine the optimal solution to dissolve mucus from the intestine in situ, washed intestinal tubules were filled with 1 M HCl, PBS, or 1 M NaOH for 24 h (Figure 1C). Before treatment, the intestinal lining was undamaged, and mucus was tightly bound to the lining (Figure 1C, left). The pH of the solvating solution affected the appearance of the intestine and the mucus layer (Figures 1C and 1D) and extent of solvation (Figure 1E). Filling the intestinal tubules with an acidic solution (1 M HCl) for 24 h turned the mucus layer into a whitish gel and the tissue became rigid (Figure 1D, middle left). A neutral solution (saline) only partially solubilized the mucus layer (Figure 1D, middle right). An alkaline solution (1 M NaOH) dissolved most of the mucus layer and turned the viscera semisolid (Figure 1D, right). The total amount of protein in the alkaline solution was significantly higher ($P < 0.05$) than in the HCl and PBS solutions (Figure 1E).

The concentration of the alkaline solution affected the amount of protein recovery and the extent of tissue damage (Figures 1F–H). Treatment with HCl (Figure 1F, middle left) caused some tissue damage, compared to untreated controls (Figure 1F, left). Treatment with PBS

did not significantly affect the epithelial tissue, which retained much of the villous architecture of untreated tissue (Figure 1F, middle right and inset). At a strength of 1 M NaOH, the underlying epithelial tissue showed some damage and individual villi were difficult to identify (Figure 1F, right). Treatment with a lower concentration of NaOH (0.01 M), compared to 1 M NaOH, reduced epithelial damage and retained villous architecture (Figure 1G). Treatment with 0.1 M NaOH, produced comparable amounts of recovered protein to treatment with 1 M NaOH (Figure 1H). The amount of recovered protein significantly decreased after treatment with NaOH solutions of lower concentration (0.01 M and below; $P < 0.05$; Figure 1H).

The amount of cellular contaminant proteins in the extracted mucus was reduced by exploiting the reversible, pH-dependent sol–gel transition of mucin (Figure 1I). After intestinal mucus was solubilized in 0.01 M NaOH, it was purified by a pH adjustment step. The acidity of the solution was reduced to a pH of 4.0 and then increased to a value of 8.0. When the pH was reduced, a gel formed (Figure 1B), enabling the supernatant to be removed. One cycle of this pH-adjustment process reduced the total protein in the extract by 40% ($P < 0.05$), but repeated sol–gel cycles did not significantly change the protein content (Figure 1I). Four sol–gel cycles were needed to reduce the DNA content by 30% ($P < 0.05$; Figure 1J). DNA contamination was reduced significantly by DNase treatment ($P < 0.05$; see Figure S1 in the Supporting Information). The removed supernatant did not gel at pH 4.0. After dialysis and lyophilization, the entire process generated 1274 ± 49 mg of dry protein per meter of intestine. The theoretical amount of mucus in the intestine was calculated to be 1775 mg/m, accounting for the increase in cross-sectional surface area due to plicae circularis and villi structure (see Figure S2 in the Supporting Information)^{55,56}. Compared to this theoretical value, PSIM extraction had a yield of 71.75%. The final product reconstituted in a buffer medium was termed porcine small intestinal mucus (PSIM).

Reconstituted PSIM Preserves Reversible pH Dependence.

The pH of PSIM affected its appearance, absorbance, rheological properties, and aggregation. At pH 7, reconstituted PSIM (20 mg/mL) was optically clear and became turbid at lower pH (Figure 2A, left and middle). High-concentration PSIM (80 mg/mL) was a viscous fluid that flowed in an inverted tube (Figure 2B, left tube). At pH 4, high-concentration PSIM formed a gel that retains its shape in an inverted tube (Figure 2B, right tube). The turbidity of reconstituted PSIM increased as the pH decreased until reaching a maximum at pH 4 (Figure 2C, top). This change in physical appearance matched the absorbance at 410 nm over this range (Figure 2C, bottom). Reconstituted PSIM exhibited an absorbance peak at 410 nm in the range from 290 nm to 790 nm (see Figure S3 in the Supporting Information). The absorbance at pH 4 was significantly greater than at pH 7 ($P < 0.05$) and pH 2 ($P < 0.05$; Figure 2D) and the greatest difference in absorbance was between pH 7 and pH 6 ($P < 0.05$).

The rheological properties of reconstituted PSIM matched the physical appearance and absorbance. The elastic (G') and viscous (G'') moduli were greater at pH 4 than at pH 7 ($P < 0.05$; Figure 2D), matching the gel-like behavior at low pH (Figure 2B). Further acidification to pH 2 reduced both moduli from that of pH 4 ($P < 0.05$; Figure 2D), similar

to the reduction in absorbance (Figure 2C). For all pH levels (pH 2, 4, and 7), G' was greater than G'' ($P < 0.05$), and the greatest difference (more than 4 times) was observed at pH 4 (Figure 2D). The elastic modulus was greater than the viscous modulus over the entire frequency range from 1 rad/s to 68.3 rad/s (see Figure S4 in the Supporting Information). At a microscopic level, pH affected the aggregation of PSIM (Figure 2E). At pH 7, no aggregation was observed. At pH 6 and below, microscopic aggregates were present (Figure 2E). The overall size and branching of PSIM aggregates gradually increased as the pH decreased, until reaching a pH value of 4. At pH values of 3 and lower, the size of the aggregates decreased. Area coverage increased with decreasing pH until reaching a pH value of 4 and then decreased as pH was reduced to a value of pH 2 (Figure 2F). The pH affected the physical properties of PSIM similarly. Each had its highest value at pH 4. Absorbance correlated positively with the viscous modulus ($R^2 = 0.95$), the elastic modulus ($R^2 = 0.90$), and the area coverage ($R^2 = 0.9998$).

The pH-dependent change in absorbance was reversible. As the pH of a PSIM solution was rapidly changed from 8 to 4 and back to 8 (Figure 2G), the solution went from clear to turbid and back to clear (see Figure 2A, as well as Movie S3 in the Supporting Information). When this reversibility was quantified using absorbance measurements and smaller pH intervals, the results matched the observed changes in turbidity. Decreasing the pH of the PSIM solution from 8 to 4 increased absorbance and it returned to a similar value as the pH was increased back to 8 (Figure 2G).

Barrier Function of PSIM Is pH-Dependent.

The mucus barrier function changed with the pH and aggregation of PSIM. When a bacterial solution was applied to a transwell membrane covered in PSIM, transmigration of the bacteria resulted in an increase in bacterial density in the bottom well as a function of time (see Figures 3A and 3B). Two species of bacteria, *Escherichia coli* (Figure 3A) and *Salmonella enterica* serovar Typhimurium (Figure 3B), both transmigrated through mucus. PSIM at pH 7, which had not formed a gel, significantly slowed *E. coli* transmigration, compared to a PSIM-free control ($P < 0.05$; Figure 3C). *Salmonella* transmigration was not affected by the presence of PSIM at pH 7 (Figure 3B). At pH 4, the aggregated PSIM significantly decreased transmigration of both bacteria ($P < 0.05$). At pH 2, bacterial transmigration was significantly reduced compared to pH 7, while more bacteria migrated across the mucus barrier compared to that observed at pH 4 ($P < 0.05$). These effects on bacterial transmigration were significant at all time points (Figures 3A and 3B) and were inversely correlated with PSIM aggregation ($R^2 = -0.97$ for *E. coli* and $R^2 = -0.99$ for *Salmonella*; compare Figures 3C and 3D to 2F).

PSIM affected the motility of both *Salmonella* and *E. coli* at low pH (see Figures 3E–H, as well as Movies S1 and S2 in the Supporting Information). In PSIM at pH 7, the average speeds of *E. coli* and *Salmonella* were not different from PSIM-free controls (Figure 3F). At pH 4, aggregated PSIM significantly decreased the motility of both species; the speeds of *E. coli* and *Salmonella* were slowed by 370% and 40%, respectively, compared to controls ($P < 0.05$; see Figure 3F). In PSIM at pH 7, both bacterial species were in a free-swimming state. In both aqueous controls and neutral pH PSIM, more than 80% of the bacteria were motile

with speeds of at least 2 $\mu\text{m/s}$ (Figures 3G and 3H). In aggregated PSIM at pH 4, the bacteria were immobilized. At pH 4, the presence of PSIM increased the percentage of nonmotile *Salmonella* and *E. coli* with speeds of $<2 \mu\text{m/s}$, from 35% to 54% and 12% to 87%, respectively ($P < 0.05$). *Salmonella* were more motile than *E. coli* in PSIM at pH 4; there were fewer immobilized bacteria (speed $<2 \mu\text{m/s}$; $P < 0.05$) and more moderately motile bacteria (speed = 2–4 $\mu\text{m/s}$; $P < 0.05$). The effect of pH on motility indicates how pH affected bacterial migration through layers of PSIM (see Figures 3A–D).

Calcium Regulates PSIM at Neutral pH.

Calcium affected the microscopic and macroscopic properties of PSIM. The addition of calcium at neutral pH increased the visible turbidity and absorbance of PSIM in a similar manner to reducing pH (Figure 4). At pH 7, PSIM was optically clear. Increasing the Ca^{2+} concentration proportionally increased the turbidity (Figure 4A). At pH 4, increasing the Ca^{2+} concentration had no effect on the turbidity of PSIM. Similar to pH, absorbance at 410 nm matched the turbidity. At pH 7, increasing the Ca^{2+} concentration significantly increased PSIM absorbance ($P < 0.05$), whereas, at pH 4, increasing the Ca^{2+} concentration did not affect the absorbance (Figure 4B). The effect of calcium on absorbance was reversible. The addition of calcium chelating EDTA reduced the absorbance that increased in response to the addition of calcium ($P < 0.05$; see Figure 4C, as well as Movie S4 in the Supporting Information).

Calcium caused similar microscopic changes to PSIM as acidic pH. Small aggregates formed at pH 7 with 1 mM Ca^{2+} (Figure 4D), whereas no aggregates formed without Ca^{2+} (Figure 2E). With 1 mM Ca^{2+} , area coverage increased with pH until a value of 4 and then decreased (Figure 4E) with a similar pattern to PSIM without calcium (Figure 2F). The effect of calcium was greatest at neutral pH. The addition of 1 mM Ca^{2+} significantly increased ($P < 0.05$) the area coverage (Figure 4E), compared to PSIM without calcium (see Figures 4E (inset) and 2F).

Calcium Controls the Thickness and Porosity of the Mucus Barrier.

At neutral pH, the Ca^{2+} concentration affected the thickness and permeability of PSIM. When the Ca^{2+} concentration was 5 mM and above, PSIM formed visible layers after overnight incubation as aggregated mucins precipitated (arrows in Figure 5A). No layers formed when the Ca^{2+} concentration was 1 mM. The thicknesses of the mucus layers increased linearly with Ca^{2+} concentration ($P < 0.05$; Figure 5B). The mucus layers formed at different Ca^{2+} concentrations affected the transport of fluorescent FITC-dextran in an unexpected manner (see Figures 5C and 5D); the lowest transport was not observed in the thickest layer. The FITC-dextran concentration, which resulted from diffusion through PSIM layers, increased with time (Figure 5C). FITC-dextran transport was highest at 1 mM Ca^{2+} , where there was no visible PSIM barrier ($P < 0.05$; see Figure 5D). Transport was lowest at 5 mM Ca^{2+} ($P < 0.05$). At Ca^{2+} concentrations of 10 and 20 mM, the transport of FITC-dextran was greater than that observed at 5 mM, even though the barriers were thicker ($P < 0.05$; see Figure 5D). This pattern was consistent for all time points (Figure 5C).

The differences in diffusion for the PSIM layers formed with different levels of Ca^{2+} was caused by its microscopic structure. Calcium affected the size of PSIM aggregates, the spacing between them, and the total area of aggregated material. In the presence of 1 mM Ca^{2+} , PSIM formed microscopic aggregates, 2–5 μm in diameter (Figure 6A). In 5 mM Ca^{2+} , there were more aggregates of approximately the same size. At 10 and 20 mM Ca^{2+} , PSIM formed larger, branched aggregates (arrows in Figure 6A). At 5 mM Ca^{2+} , the aggregates were closest (Figure 6B). Most of the spaces (>95%) between the aggregates were <5 μm in size, which was significantly greater than the aggregate spacing for 1 mM ($P < 0.05$). At 1 mM Ca^{2+} , approximately half (49.8%) of the spaces were 5–10 μm , which was significantly greater than the percentage of spaces at 5 mM (~5%; $P < 0.05$). At 10 and 20 mM Ca^{2+} , there were more large spaces (15–20 and 20–25 μm) between aggregates than observed at 1 and 5 mM ($P < 0.05$). At these higher Ca^{2+} concentrations, PSIM aggregates formed islands with low interparticle distances (<5 μm) and longer distances (>5 μm) between islands (Figure 6A). These large spaces between islands created pores through the PSIM layers. At 1 mM Ca^{2+} , ~3% of the surface area was covered by PSIM aggregates (Figure 6C). Increasing the Ca^{2+} concentration to 5 mM increased the area covered 15-fold ($P < 0.05$). Further increase in the Ca^{2+} concentration to 10 mM reduced the area coverage to 18%. Similar to the aggregate distribution, no significant difference in the area coverage was observed if the Ca^{2+} concentration was increased from 10 mM Ca^{2+} to 20 mM Ca^{2+} .

Molecular retention within PSIM layers was dependent on Ca^{2+} concentration (see Figures 6D–G). As with the transmitted light measurements (Figure 6A), the size of PSIM aggregates increased as the Ca^{2+} concentration increased (see Figure 6D). Green fluorescence from FITC-dextran, which indicates the location of molecules retained in the PSIM layers, became patchy as the Ca^{2+} concentration increased (Figure 6D). With an increase in calcium concentration from 1 mM to 5 mM, the average GFP fluorescence decreased ($P < 0.05$; Figure 6E), indicating a decrease in the number of molecules retained in the PSIM layer. A further increase in calcium concentration to 10 mM reversed this direction and increased the average GFP fluorescence ($P < 0.05$; Figure 6E). The local structure of the PSIM aggregates explains this behavior (Figure 6F). Regions of high PSIM aggregation (stars in Figure 6F) had low GFP intensities. Pores in the PSIM layer, identified as regions with low red fluorescence (dashed circles in Figure 6F), had high GFP fluorescence. The GFP intensity in the pores was greater than in the aggregated material ($P < 0.05$; Figure 6G), indicating exclusion from PSIM aggregates.

DISCUSSION

We have developed a new method for isolating mucus from the porcine intestine (Figure 1). This method dissolves the mucus layer from intact intestines using NaOH. A dilute (0.01 M) solution was used because it dissolved most of the mucus layer (see Figures 1E and 1G) and caused minimal damage to the epithelial cell layer (Figure 1F). Minimizing the damage reduced the amount of contaminating proteins in the purified mucus (Figure 1G). A sol-to-gel transition in the extraction method (Figure 1H) eliminated pH-unresponsive macromolecules and cellular proteins without the use of high-cost instrumentation. Solubilized mucus proteins were recovered with a yield of 1274 mg per meter length of small intestine. The biophysical and biochemical properties of the produced mucus are

consistent with those reported previously.^{17,25,29,40} At acidic pH values, PSIM becomes more gel-like, with increasing viscous and elastic moduli (Figure 2D). With increasing concentrations of calcium, the extent of PSIM aggregation at neutral pH increases (Figure 4B). The thickness of the PSIM layer formed in the in vitro mucus model has a thickness comparable to the mucus layer in the small intestine¹⁷ (Figure 5B).

This new process has several advantages over other methods. Compared to direct scraping of mucus from the epithelial lining, solubilization of mucus greatly simplifies the extraction process. Dissolving mucus in dilute NaOH and purifying with a sol-gel transition significantly decreases contamination with cellular debris (Figure 1G). In immunogenic experiments, contamination with cellular or bacterial components could cause unwanted responses. In addition, the process is scalable and can be applied to entire lengths of PSI tubes simultaneously. Compared to commercial mucin, PSIM retains the rheological properties of natural mucus. Commercial mucins do not form a gel (see Figure S5 in the Supporting Information), which limits their use as a barrier in experiments in vitro.⁵⁷ Compared to mucin extraction protocols, this process does not require extensive downstream equipment.^{47,48} Most of these methods are limited by the quantity and yield of mucus that can be produced, which prevents the widespread use of mucus in research.

The extraction of large volumes of mucus enabled many of its properties to be quantified. An important property that was observed was the reversibility of pH and calcium-induced aggregation and gelation (see Figures 2G and 4C). Reversibility suggests that the properties of mucus respond to conditions in the local environment. This dynamic change was easily monitored because the absorbance at 410 nm was directly correlated to the degree of aggregation (see Figures 2C and 2F) and the viscous and elastic moduli (Figure 2D). Reconstituted PSIM retained the ability to be a barrier to bacterial penetration (Figure 3) and this property was dependent on pH. At neutral pH, mucus only minimally prevented penetration, but when the mucus aggregated at lower pH, penetration was considerably reduced (see Figures 3A–D). The aggregation of the mucus at pH 4 appeared to slow penetration, because the bacteria became immobilized in aggregated mucus (recall Movies S1 and S2). A gel layer of PSIM can act like a natural barrier by controlling molecular diffusion and bacterial transmigration.

Another observation was that calcium plays a critical role in the intestinal milieu. Similar to pH, the availability of Ca^{2+} ions affected the thickness of the mucus layer (Figure 5B). Increasing the calcium concentration increased PSIM aggregation, suggesting that calcium affected PSIM via mechanisms similar as changes in pH. In addition, there was an interplay between the responses of mucus to pH and calcium. Overall, acidic pH had a greater effect on mucus aggregation than calcium concentration within the physiological range (Figure 4B). At neutral pH and in the absence of calcium, mucus was not aggregated. Increasing the calcium concentration increased mucus aggregation but did not reach the same extent as that observed at pH 4 (Figure 4B). Calcium-driven aggregation also affected the barrier function. From low (5 mM) to high (20 mM) physiological levels of calcium,^{35,37} the molecular permeability of mucus increased (see Figure 5C).

The microscopic structure of mucus explains how calcium controls the barrier function of mucus. The primary microscopic features that affects the physical properties of mucus are the arrangement and density of aggregates. At very low calcium levels (1 mM), mucus aggregation is minimal (Figure 6A). At low physiological calcium concentrations (5 mM), small and uniform aggregates begin to appear. At higher calcium concentrations (10–20 mM), larger, more branched aggregates form. The branching of mucin aggregates did not increase once Ca^{2+} concentration was higher than 10 mM. Although the density of aggregates increases, this condensation decreases the surface area coverage (Figure 6C). The branched nature of the aggregates formed void spaces in the mucus layer (Figure 6D) that increase molecular diffusion while also increasing the thickness of the layer (Figure 5A). The structure and extent of these aggregates explains how calcium increased both mucus layer thickness and molecular transport.

These effects suggest how the local calcium concentration controls the properties of the mucus barrier (Figure 7). The increased concentration of ionic molecules after ingesting food (predominantly calcium) induce mucin aggregation and increases the thickness of the mucus barrier. The increased aggregation increases molecular permeability (Figure 6), while simultaneously increasing resistance to microbial penetration from the lumen. If the behavior of PSIM in high calcium is similar to pH 4, where both had considerable aggregation (Figure 4B), then PSIM aggregation at high calcium would also have high resistance to microbial penetration from the lumen (see Figures 3 and 5). Therefore, dense branched aggregates increase the open channels for molecular diffusion while also creating a network to ensnare invasive microbes. As the mucus flows along the epithelium, its viscoelastic and barrier properties change, in response to the lumen content. Because the properties of the mucus are reversible, it is instantaneously responsive and serves different functions in different intestinal environments, e.g., an empty lumen and one directly after eating.

CONCLUSION

A high-throughput method to extract natural mucus will stimulate broad aspects of mucus barrier research. Using mucus extracted with this process, we have shown that the local ionic environment plays an important role in regulating the biophysical properties of the mucus barrier. The techniques presented here will help uncover the mechanisms behind the effects of environmental molecules on biophysical properties of mucus. The in vitro mucus barrier model is functional and can be tuned to match physiological thicknesses and densities of native mucus. We envision that these models will serve as high-throughput tools for understanding the role of the mucus barrier in nutrient absorption, host–microbiome interactions, and drug absorption. In addition, similar methods can be applied to other mucosal tissues, including the lung, cervix, and vagina. Ultimately, a better understanding of mucus barriers and their interaction with the local environment has the potential to improve treatment of intestinal diseases and other mucosal barrier organs.

MATERIALS AND METHODS

Natural Mucin Extraction from a Porcine Small Intestine.

Small intestines from freshly slaughtered pigs were obtained from a local slaughterhouse and transported to the laboratory on ice within 2 h. Porcine small intestines (PSIs) were cut into segments 6 in. long and washed with running deionized (DI) water. The tissues were filled with 50 mL of 1 M HCl, 1× PBS, and 1 M NaOH. After both ends are tied, PSI tubules were incubated at 4 °C for 24 h. The solutions were collected and aliquoted into 1 mL Eppendorf tubes and centrifuged in a microcentrifuge at 10 000*g* for 30 min. The supernatant was collected, and total protein was quantified using a Bradford assay. Bovine serum albumin was used as a standard for known protein concentration. For optimization of NaOH concentration, cleaned PSIs (6-in., *n* = 3) were filled with 10 mL of serially diluted NaOH solutions (1, 0.1, 0.01, and 0.001 M) and incubated at 4 °C for 24 h. The solutions were collected and stored at –80 °C. To quantify total soluble protein, the frozen solutions from all four conditions were thawed at 4 °C, vortexed thoroughly, and divided into 1 mL aliquots. The aliquots were centrifuged in a microcentrifuge at 10 000*g* for 30 min. Supernatant from three aliquots were dialyzed against DI water in a cellulose membrane (molecular size cutoff = 14 kDa) for 72 h at 4 °C with a water change every 12 h. The dialyzed solution was lyophilized to quantify the dry mucus weight and reconstituted at an equal concentration in DI water to quantify the total protein content, using a Bradford assay.

For the scaleup, PSIs (2 m) were flushed with running tap water to remove the luminal content and the loosely bound mucus layer. The luminal space was then filled with 350 mL of 0.01 M NaOH with both ends tied and incubated at 4 °C for 24 h. The solubilized mucus extract was collected and centrifuged at 20 000*g* for 2 h at 4 °C to precipitate debris in 50 mL tubes. After collecting the clear supernatant, the pH was adjusted to 4 to induce PSIM aggregation. Aggregated PSIM was separated by centrifugation at 200*g* for 15 min and resuspended to get a clear solution in sterile DI water by adjusting pH to 8.0–8.5. The solubilized PSI was filtered through a 40 μ m strainer and dialyzed (molecular size cutoff = 14 kDa). The dialyzed mucus extract was sterilized by adding 1% (v/v) chloroform under constant stirring at 4 °C for 72 h. The sterile solution at pH ~7 was frozen at –80 °C, lyophilized, and stored as a powder at –20 °C until used. All of the experiments were conducted using the lyophilized powder reconstituted in an appropriate buffer or cell culture medium, and the term “PSIM” is used to denote the reconstituted form at a known concentration. The theoretical density of mucin protein in the intestine was calculated by considering the increase in surface area that was due to the intestinal folds and the villous architecture (see Figure S1 in the Supporting Information).

Histology.

Tissues were cut into 2-cm sections and excess water was removed. Tissues were embedded in optimum cutting temperature (OCT) cryomatrix and snap frozen in liquid nitrogen. Using a cryostat (Thermo Scientific, CRYOSTARNX70), frozen tissues were sectioned at a thickness of 20 μ m. Sections were fixed with 10% formalin and stained with hematoxylin and eosin (H&E).

Biophysical Characterizations of the Reconstituted Mucus.

Rheological Characterization.—Bulk rheology on reconstituted PSIM samples from three different pig intestines was conducted. Small amplitude oscillatory shear measurements were performed in a Kinexus Pro rheometer (Malvern Instruments, U.K.) using a cuvette cell geometry. PSIM samples were loaded into the cup at pH values of 2, 4, and 7 and held at a constant temperature of 37 °C. Oscillatory frequency sweeps were conducted between 1 and 100 Hz at a constant strain of 0.25%.

Absorbance Characterization.—PSIM aggregation was quantified using ultraviolet–visible light (UV-vis) spectroscopy. The absorbance value at 410 nm was used as a measure of PSIM aggregation. Lyophilized PSIM powder was reconstituted in 20 mM HEPES at pH 7. The pH value of the reconstituted PSIM was adjusted using 2 M HCl and 2 M NaOH. 100 μL of PSIM samples were added to a 96-well plate, and the absorbance was measured using a microplate reader (Synergy H1, BioTek).

Microscopic Characterization of PSIM Aggregates.—Twenty microliter (20 μL) droplets of PSIM solution were placed between glass coverslips and clear glass slides and were imaged using a bright-field microscope (EVOS). The images were binarized using a built-in scheme in the image analysis software (ImageJ). The area covered by aggregates per image was quantified and plotted as percentage area covered normalized by the total area of the image.

Dynamic Viscoelastic Characterization.—PSIM 2% (w/v) at pH 7.3 was added to a glass vial and subjected to constant stirring. The pH was monitored in real time using a needle-type pH probe (PreSens) and was adjusted using 2N HCl and 2N NaOH solutions. Samples were collected at specific pH values for UV absorbance measurements.

Bacterial Cell Culture.—Two bacterial strains *S. typhimurium* (SL1344) and *E. coli* (MG1655) were used for live bacterial experiments. Frozen stocks of the bacterial strains were inoculated in Luria Broth (LB) and grown overnight. Optical density at 600 nm (OD600) of the overnight cultures was measured and the bacteria were seeded at a density of 1×10^7 in fresh LB medium and allowed to grow to an OD600 of 0.6–0.8 and used for further experiments.

Two-Dimensional (2D) Bacterial Motility Assay in PSIM on a Glass Slide.—Live bacterial imaging was performed in a hanging drop assembly for bacterial motility quantification. Bacteria cultured in LB were diluted 1:10 in PSIM (2% w/v) or control (20 mM HEPES solution), and a 2 μL droplet was added on top of a circular cover glass. The cover glass with the droplet was inverted and rested on top of a 1-mm-thick PDMS ring bound to a glass slide. The glass slide with the hanging drop was imaged using an inverted fluorescent microscope (Zeiss). Bacterial movement was tracked in a single 2D plane and the average speed was quantified using the in-built particle tracker plug-in “Trackmate” in ImageJ software.

Three-Dimensional (3D) Bacterial Diffusion Assay through PSIM in a Transwell Insert.—HEPES solution (20 mM) was added to transwell inserts (50 μL /transwell) and used as the no-barrier condition and compared to 50 μL of PSIM 2% (w/v) at pH 2, 4, and 7. Transwell inserts were placed into the wells of a 24-well plate containing 600 μL of LB. A 100 μL of live bacterial culture (10^{11} cells/mL) was gently added to the insets, and the plates were incubated at 37 °C and 5% CO_2 . Fluorescence intensity was measured at 1-h intervals for 6 h in the bottom well and converted to colony forming units (CFUs), using a previously established standard curve.

Fixation and Cryosectioning of PSIM Layers on Transwell Membranes.—

Transwell inserts with different PSIM gel layers formed in response to added Ca^{2+} were held vertical. A small cut was created on the edge of the membrane from the bottom side. The inserts were kept on tissue paper, to absorb all liquid from the membrane and mucin gel. Transwell inserts were transferred into wells of 24 well plate containing 600 μL of 10% formalin solution in PBS. Formalin (10% in phosphate buffered saline) solution was gently added on the apical side of the transwell and kept at room temperature for 10 min. Inserts were moved to a different well and the formalin solution was carefully replaced by PBS three times on apical and basal sides. The membranes were dehydrated again using tissue paper and carefully cut out from the inserts using a scalpel. The membranes were embedded in OCT and snap-frozen in liquid nitrogen. Frozen membranes were cross-sectioned at a 10 μm thickness using a cryostat and collected on glass slides. The sections were imaged using a bright-field microscope (EVOS) and the thickness of the gel layers was calculated using ImageJ software.

Lectin Staining for Visualization of PSIM Aggregates.—Far-red-fluorescence (Cy5)-conjugated *Sambucus nigra* (SNA) lectins (Vector Laboratories) were added to PSIM 2% (w/v) at a final concentration of 10 $\mu\text{g}/\text{mL}$ and incubated at room temperature for 30 min. The solution was dialyzed against DI water for 24 h constant stirring in a darkroom at 4 °C. The fluorescent lectin tagged PSIM was used to visualize PSIM aggregates using fluorescence microscopy.

Pore Size Distribution.—Aggregates were imaged microscopically in PSIM (2% w/v) containing 1, 5, 10, and 20 mM Ca^{2+} . Interaggregate distance was measured at 100 random locations per image using ImageJ software. An average number distribution (expressed as a percentage) of at least five independent images from each condition was plotted in a range of 0–30 μm . FITC-dextran diffusion was measured at different calcium concentrations. HEPES solution (20 mM) was added to the wells of a 24-well plate (600 μL /well). PSIM solution 2% (w/v) in 20 mM HEPES at a pH of 7 and containing 1, 5, 10, and 20 mM Ca^{2+} was added to transwell inserts (100 μL /transwell). Transwell inserts were placed into the wells of 24-well plates containing 600 μL of HEPES solution, and the well plate was incubated for 12 h at 37 °C and 5% CO_2 , to allow for mucus layer formation. A 10 μL droplet of 10 mg/mL solution of FITC dextran (molecular weight of 20 kDa) in DI water was gently added to the insets and the plate was incubated at 37 °C and 5% CO_2 . Fluorescence intensity was measured at 1-h intervals for 6 h in the bottom well and converted to a concentration of FITC dextran.

Fluorescent Imaging and Area Overlap Analysis.—PSIM 2% (w/v) at pH 7 and containing 1, 5, 10, and 20 mM Ca²⁺ was added to a 96-well plate (100 μ L/well). The well plate was incubated overnight at 37 °C and 5% CO₂ to allow for mucus layer formation. FITC-dextran (MW = 20 kDa) at a concentration of 10 mg/mL in 20 mM HEPES was gently added to the transwells (10 μ L/transwell) and the plate was incubated at 37 °C and 5% CO₂. Fluorescent images were captured using a Zeiss Axiovert 4-laser spinning disc confocal microscope (20 \times magnification) after 1 h. Image analysis for GFP intensity (FITC-dextran) and RFP intensity (Cy5 lectin tagged PSIM) was performed using ImageJ software and normalized for the total area of the images. Areas with bright RFP intensity were considered as “aggregates” and those with low RFP intensity areas were considered to be “pores”. The average intensity of FITC was determined in the entire image and in the pore and aggregate regions.

Statistical Analysis.—A two-tailed Student’s *t*-test assuming unequal variances was used for statistical analysis of different conditions. One-way ANOVA with Bonferroni posthoc test was used for multiple comparisons. Differences were considered significant at *p* < 0.05. All data are presented as a mean \pm standard deviation.

All chemicals and supplies were purchased from Fisher Scientific and Sigma–Aldrich, unless otherwise specified.

Supplementary Material

Refer to Web version on PubMed Central for supplementary material.

ACKNOWLEDGMENTS

We thank Dr. Henning Winter for valuable discussions of rheological characterization and Dr. Shelly Peyton for assistance with confocal microscopy. This work was supported by the National Cancer Institute (No. R00 CA163671, to J.L.; No. R01CA188382, to N.S.F.), Institute for Applied Life Sciences, and Department of Chemical Engineering. K.W.K. was supported by the National Research Service Award (No. T32 GM008515) from the National Institutes of Health.

REFERENCES

- (1). Allen A; Bell A; Mantle M; Pearson JP, The Structure and Physiology of Gastrointestinal Mucus. In Mucus in Health and Disease—II; Chantler EN, Elder JB, Elstein M, Eds.; Springer: Boston, MA, 1982; pp 115–133.
- (2). Cone RA Barrier properties of mucus. *Adv. Drug Delivery Rev* 2009, 61 (2), 75–85.
- (3). Johansson ME; Sjoval H; Hansson GC The gastrointestinal mucus system in health and disease. *Nat. Rev. Gastroenterol. Hepatol* 2013, 10 (6), 352–61. [PubMed: 23478383]
- (4). Turner JR Intestinal mucosal barrier function in health and disease. *Nat. Rev. Immunol* 2009, 9 (11), 799–809. [PubMed: 19855405]
- (5). Lieleg O; Ribbeck K Biological hydrogels as selective diffusion barriers. *Trends Cell Biol.* 2011, 21 (9), 543–51. [PubMed: 21727007]
- (6). Alipour M; Zaidi D; Valcheva R; Jovel J; Martinez I; Sergi C; Walter J; Mason AL; Wong GK; Dieleman LA; Carroll MW; Huynh HQ; Wine E Mucosal Barrier Depletion and Loss of Bacterial Diversity are Primary Abnormalities in Paediatric Ulcerative Colitis. *J. Crohns Colitis* 2016, 10 (4), 462–71. [PubMed: 26660940]
- (7). Ijssennagger N; van der Meer R; van Mil SW Sulfide as a Mucus Barrier-Breaker in Inflammatory Bowel Disease? *Trends Mol. Med* 2016, 22 (3), 190–9. [PubMed: 26852376]

- (8). Swidsinski A; Weber J; Loening-Baucke V; Hale LP; Lochs H Spatial Organization and Composition of the Mucosal Flora in Patients with Inflammatory Bowel Disease. *Journal of Clinical Microbiology* 2005, 43 (7), 3380–3389. [PubMed: 16000463]
- (9). Ehre C; Ridley C; Thornton DJ Cystic fibrosis: An inherited disease affecting mucin-producing organs. *Int. J. Biochem. Cell Biol* 2014, 52, 136–145. [PubMed: 24685676]
- (10). Krishn SR; Kaur S; Smith LM; Johansson SL; Jain M; Patel A; Gautam SK; Hollingsworth MA; Mandel U; Clausen H; Lo WC; Fan WT; Manne U; Batra SK Mucins and associated glycan signatures in colon adenoma-carcinoma sequence: Prospective pathological implication(s) for early diagnosis of colon cancer. *Cancer Lett.* 2016, 374 (2), 304–14. [PubMed: 26898938]
- (11). Velcich A; Yang W; Heyer J; Fragale A; Nicholas C; Viani S; Kucherlapati R; Lipkin M; Yang K; Augenlicht L Colorectal Cancer in Mice Genetically Deficient in the Mucin Muc2. *Science* 2002, 295 (5560), 1726–1729. [PubMed: 11872843]
- (12). Bansil R; Celli JP; Hardcastle JM; Turner BS The Influence of Mucus Microstructure and Rheology in *Helicobacter pylori* Infection. *Front. Immunol* 2013, 4, 310. [PubMed: 24133493]
- (13). Kleessen B; Kroesen AJ; Buhr HJ; Blaut M Mucosal and Invading Bacteria in Patients with Inflammatory Bowel Disease Compared with Controls. *Scand. J. Gastroenterol* 2002, 37 (9), 1034–1041. [PubMed: 12374228]
- (14). Ambort D; Johansson ME; Gustafsson JK; Nilsson HE; Ermund A; Johansson BR; Koeck PJ; Hebert H; Hansson GC. Calcium and pH-dependent packing and release of the gel-forming MUC2 mucin. *Proc. Natl. Acad. Sci. U. S. A* 2012, 109 (15), 5645–50. [PubMed: 22451922]
- (15). Tytgat KM; Buller HA; Opdam FJ; Kim YS; Einerhand AW; Dekker J Biosynthesis of human colonic mucin: Muc2 is the prominent secretory mucin. *Gastroenterology* 1994, 107 (5), 1352–63. [PubMed: 7926500]
- (16). Dekker J; Rossen JWA; Büller HA; Einerhand AWC The MUC family: an obituary. *Trends Biochem. Sci* 2002, 27 (3), 126–131. [PubMed: 11893509]
- (17). Atuma C; Strugala V; Allen A; Holm L The adherent gastrointestinal mucus gel layer: thickness and physical state in vivo. *American Journal of Physiology - Gastrointestinal and Liver Physiology* 2001, 280 (5), G922–G929. [PubMed: 11292601]
- (18). Vaishnav S; Yamamoto M; Severson KM; Ruhn KA; Yu X; Koren O; Ley R; Wakeland EK; Hooper LV The antibacterial lectin RegIII γ promotes the spatial segregation of microbiota and host in the intestine. *Science (Washington, DC, U. S.)* 2011, 334 (6053), 255–258.
- (19). Cornick S; Tawiah A; Chadee K Roles and regulation of the mucus barrier in the gut. *Tissue Barriers* 2015, 3 (1–2), e982426. [PubMed: 25838985]
- (20). Tlaskalova-Hogenova H; Stepankova R; Kozakova H; Hudcovic T; Vannucci L; Tuckova L; Rossmann P; Hrnecir T; Kverka M; Zakostelska Z; Klimesova K; Pribylova J; Bartova J; Sanchez D; Fundova P; Borovska D; Srutkova D; Zidek Z; Schwarzer M; Drastich P; Funda DP The role of gut microbiota (commensal bacteria) and the mucosal barrier in the pathogenesis of inflammatory and autoimmune diseases and cancer: contribution of germ-free and gnotobiotic animal models of human diseases. *Cell. Mol. Immunol* 2011, 8 (2), 110–20. [PubMed: 21278760]
- (21). Faderl M; Noti M; Corazza N; Mueller C Keeping bugs in check: The mucus layer as a critical component in maintaining intestinal homeostasis. *IUBMB Life* 2015, 67 (4), 275–85. [PubMed: 25914114]
- (22). Johansson ME; Phillipson M; Petersson J; Velcich A; Holm L; Hansson GC The inner of the two Muc2 mucin-dependent mucus layers in colon is devoid of bacteria. *Proc. Natl. Acad. Sci. U. S. A* 2008, 105 (39), 15064–9. [PubMed: 18806221]
- (23). Birchenough GM; Nystrom EE; Johansson ME; Hansson GC A sentinel goblet cell guards the colonic crypt by triggering Nlrp6-dependent Muc2 secretion. *Science* 2016, 352 (6293), 1535–42. [PubMed: 27339979]
- (24). Kamphuis JBJ; Mercier-Bonin M; Eutamène H; Theodorou V Mucus organisation is shaped by colonic content; a new view. *Sci. Rep* 2017, 7 (1), 8527. [PubMed: 28819121]
- (25). Celli JP; Turner BS; Afdhal NH; Ewoldt RH; McKinley GH; Bansil R; Erramilli S Rheology of Gastric Mucin Exhibits a pH-Dependent Sol–Gel Transition. *Biomacromolecules* 2007, 8 (5), 1580–1586. [PubMed: 17402780]

- (26). Lafitte G; Söderman O; Thuresson K; Davies J PFG-NMR diffusometry: A tool for investigating the structure and dynamics of noncommercial purified pig gastric mucin in a wide range of concentrations. *Biopolymers* 2007, 86 (2), 165–175. [PubMed: 17345632]
- (27). Bansil R; Turner BS Mucin structure, aggregation, physiological functions and biomedical applications. *Curr. Opin. Colloid Interface Sci* 2006, 11 (2–3), 164–170.
- (28). Barz B; Turner BS; Bansil R; Urbanc B Folding of pig gastric mucin non-glycosylated domains: a discrete molecular dynamics study. *J. Biol. Phys* 2012, 38 (4), 681–703. [PubMed: 24615227]
- (29). Cao X; Bansil R; Bhaskar KR; Turner BS; LaMont JT; Niu N; Afdhal NH pH-dependent conformational change of gastric mucin leads to sol-gel transition. *Biophys. J* 1999, 76 (3), 1250–1258. [PubMed: 10049309]
- (30). Sellers LA; Allen A; Morris ER; Ross-Murphy SB The rheology of pig small intestinal and colonic mucus: weakening of gel structure by non-mucin components. *Biochim. Biophys. Acta, Gen. Subj* 1991, 1115 (2), 174–179.
- (31). Yang N; Garcia MA; Quinton PM Normal mucus formation requires cAMP-dependent HCO₃-secretion and Ca²⁺-mediated mucin exocytosis. *J. Physiol* 2013, 591 (18), 4581–93. [PubMed: 23818690]
- (32). Raynal BD; Hardingham TE; Sheehan JK; Thornton DJ Calcium-dependent protein interactions in MUC5B provide reversible cross-links in salivary mucus. *J. Biol. Chem* 2003, 278 (31), 28703–10. [PubMed: 12756239]
- (33). Verdugo P; Aitken M; Langley L; Villalon MJ Molecular mechanism of product storage and release in mucin secretion. II. The role of extracellular Ca⁺⁺. *Biorheology* 1987, 24 (6), 625–33. [PubMed: 3502764]
- (34). Fallingborg J Intraluminal pH of the human gastrointestinal tract. *Dan. Med. Bull* 1999, 46 (3), 183–196. [PubMed: 10421978]
- (35). Yildiz HM; Speciner L; Ozdemir C; Cohen DE; Carrier RL Food-associated stimuli enhance barrier properties of gastro-intestinal mucus. *Biomaterials* 2015, 54, 1–8. [PubMed: 25907034]
- (36). Fordtran JS; Locklear TW Ionic constituents and osmolality of gastric and small-intestinal fluids after eating. *Am. J. Dig. Dis* 1966, 11 (7), 503–21. [PubMed: 5937767]
- (37). Di Maio S; Carrier RL Gastrointestinal contents in fasted state and post-lipid ingestion: In vivo measurements and in vitro models for studying oral drug delivery. *J. Controlled Release* 2011, 151 (2), 110–122.
- (38). Starkey BJ; Snary D; Allen A Characterization of gastric mucoproteins isolated by equilibrium density-gradient centrifugation in caesium chloride. *Biochem. J* 1974, 141 (3), 633–9. [PubMed: 4463953]
- (39). Bell AE; Sellers LA; Allen A; Cunliffe WJ; Morris ER; Ross-Murphy SB Properties of Gastric and Duodenal Mucus: Effect of Proteolysis, Disulfide Reduction, Bile, Acid, Ethanol, and Hypertonicity on Mucus Gel Structure. *Gastroenterology* 1985, 88 (1), 269–280. [PubMed: 3917263]
- (40). Bhaskar KR; Gong DH; Bansil R; Pajevic S; Hamilton JA; Turner BS; LaMont JT Profound increase in viscosity and aggregation of pig gastric mucin at low pH. *American journal of physiology* 1991, 261 (5), G827–G832.
- (41). Li L; Lieleg O; Jang S; Ribbeck K; Han J A microfluidic in vitro system for the quantitative study of the stomach mucus barrier function. *Lab Chip* 2012, 12 (20), 4071–9. [PubMed: 22878692]
- (42). Li LD; Crouzier T; Sarkar A; Dunphy L; Han J; Ribbeck K Spatial configuration and composition of charge modulates transport into a mucin hydrogel barrier. *Biophys. J* 2013, 105 (6), 1357–65. [PubMed: 24047986]
- (43). Ho SB; Takamura K; Anway R; Shekels LL; Toribara NW; Ota H The Adherent Gastric Mucous Layer Is Composed of Alternating Layers of MUC5AC and MUC6Mucin Proteins. *Dig. Dis. Sci* 2004, 49 (10), 1598–1606. [PubMed: 15573912]
- (44). Schömig VJ; Kasdorf BT; Scholz C; Bidmon K; Lieleg O; Berensmeier S An optimized purification process for porcine gastric mucin with preservation of its native functional properties. *RSC Adv.* 2016, 6, 44932–44943.

- (45). Lai SK; O'Hanlon DE; Harrold S; Man ST; Wang Y-Y; Cone R; Hanes J Rapid transport of large polymeric nanoparticles in fresh undiluted human mucus. *Proc. Natl. Acad. Sci. U. S. A* 2007, 104 (5), 1482–1487. [PubMed: 17244708]
- (46). Boegh M; Baldursdottir SG; Mullertz A; Nielsen HM Property profiling of biosimilar mucus in a novel mucus-containing in vitro model for assessment of intestinal drug absorption. *Eur. J. Pharm. Biopharm* 2014, 87 (2), 227–35. [PubMed: 24413146]
- (47). Marshall T; Allen A The isolation and characterization of the high-molecular-weight glycoprotein from pig colonic mucus. *Biochem. J* 1978, 173 (2), 569–78. [PubMed: 697737]
- (48). Mantle M; Allen A Isolation and characterization of the native glycoprotein from pig small-intestinal mucus. *Biochem. J* 1981, 195 (1), 267–75. [PubMed: 7306053]
- (49). Sellers LA; Allen A; Morris ER; Ross-Murphy SB The rheology of pig small intestinal and colonic mucus: weakening of gel structure by non-mucin components. *Biochim. Biophys. Acta, Gen. Subj* 1991, 1115 (2), 174–9.
- (50). Davies JR; Wickstrom C; Thornton DJ Gel-forming and cell-associated mucins: preparation for structural and functional studies. *Methods Mol. Biol* 2012, 842, 27–47. [PubMed: 22259128]
- (51). Georgiades P; Pudney PDA; Thornton DJ; Waigh TA Particle tracking microrheology of purified gastrointestinal mucins. *Biopolymers* 2014, 101 (4), 366–377. [PubMed: 23955640]
- (52). Georgiades P; di Cola E; Heenan RK; Pudney PD; Thornton DJ; Waigh TA A combined small-angle X-ray and neutron scattering study of the structure of purified soluble gastro-intestinal mucins. *Biopolymers* 2014, 101 (12), 1154–64. [PubMed: 25041765]
- (53). Schömig VJ; Käs Dorf BT; Scholz C; Bidmon K; Lieleg O; Berensmeier S An optimized purification process for porcine gastric mucin with preservation of its native functional properties. *RSC Adv.* 2016, 6 (50), 44932–44943.
- (54). Schoemig V; Isik E; Martin L; Berensmeier S Solid liquid liquid extraction of porcine gastric mucins from homogenized animal material. *RSC Adv.* 2017, 7 (63), 39708–39717.
- (55). Helander HF; Fändriks L Surface area of the digestive tract – revisited. *Scand. J. Gastroenterol* 2014, 49 (6), 681–689. [PubMed: 24694282]
- (56). Varum FJ; Veiga F; Sousa JS; Basit AW Mucus thickness in the gastrointestinal tract of laboratory animals. *J. Pharm. Pharmacol* 2012, 64 (2), 218–27. [PubMed: 22221097]
- (57). Ko evar-Nared J; Kristl J; Šmid-Korbar J Comparative rheological investigation of crude gastric mucin and natural gastric mucus. *Biomaterials* 1997, 18 (9), 677–681. [PubMed: 9151999]

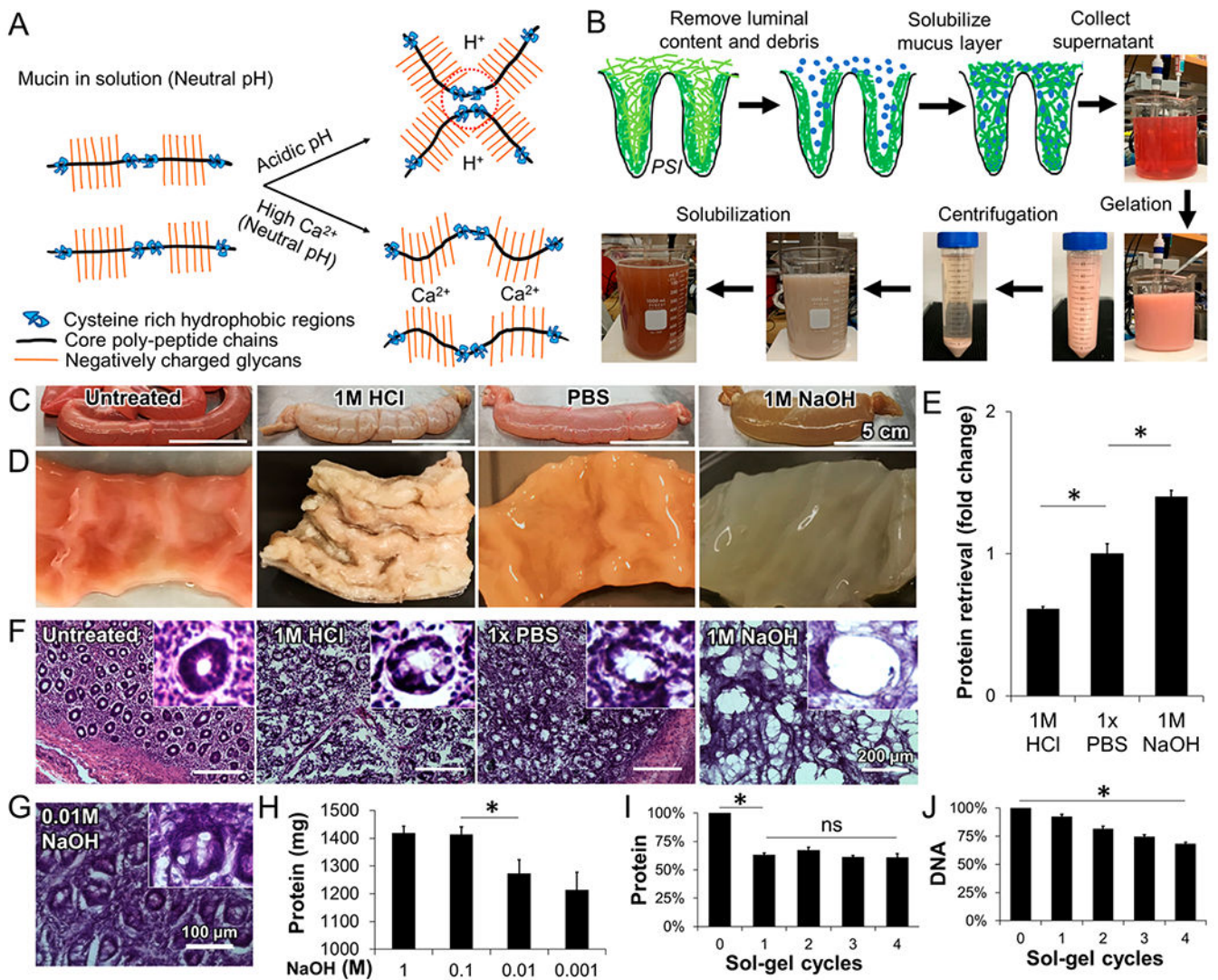


Figure 1.

Extraction of porcine small intestine mucus (PSIM). (A) Schematic of mucin microstructure, stable polymeric chains at neutral pH, hydrophobic interactions of cysteine-rich regions at acidic pH (dashed circles), and ionic interactions between calcium ions (Ca^{2+}) and negatively charged glycans at neutral pH. (B) Mucus extraction procedure starting with direct solubilization of the mucus layer with NaOH, and separation of pH responsive mucus via reversible sol-gel transition. (C) PSI tubules after 24 h of exposure to 1 M HCl, PBS, and 1 M NaOH. (D) Luminal surface of PSI tissue sections after 24 h of exposure to HCl, PBS, and NaOH. (E) Recovered protein with solutions of different pH, relative to PBS. (*, $P < 0.05$; $n = 3$.) (F) Hematoxylin and eosin (H&E)-stained histological sections of PSI tissues treated with different pH solutions. Inner panels show individual villi. (G) H&E-stained PSI section after 0.01 M NaOH treatment. (H) Total protein extracted when PSI tubules were filled with NaOH solutions ranging from 0.001 M to 1 M ($n = 3$). (I) Total protein content with repeated sol-gel cycles relative to initial total protein extracted. (J) Total DNA content

with repeated sol–gel cycles relative to the total DNA initially present in the PSIM extract.
(*, $P < 0.05$.)

Author Manuscript

Author Manuscript

Author Manuscript

Author Manuscript

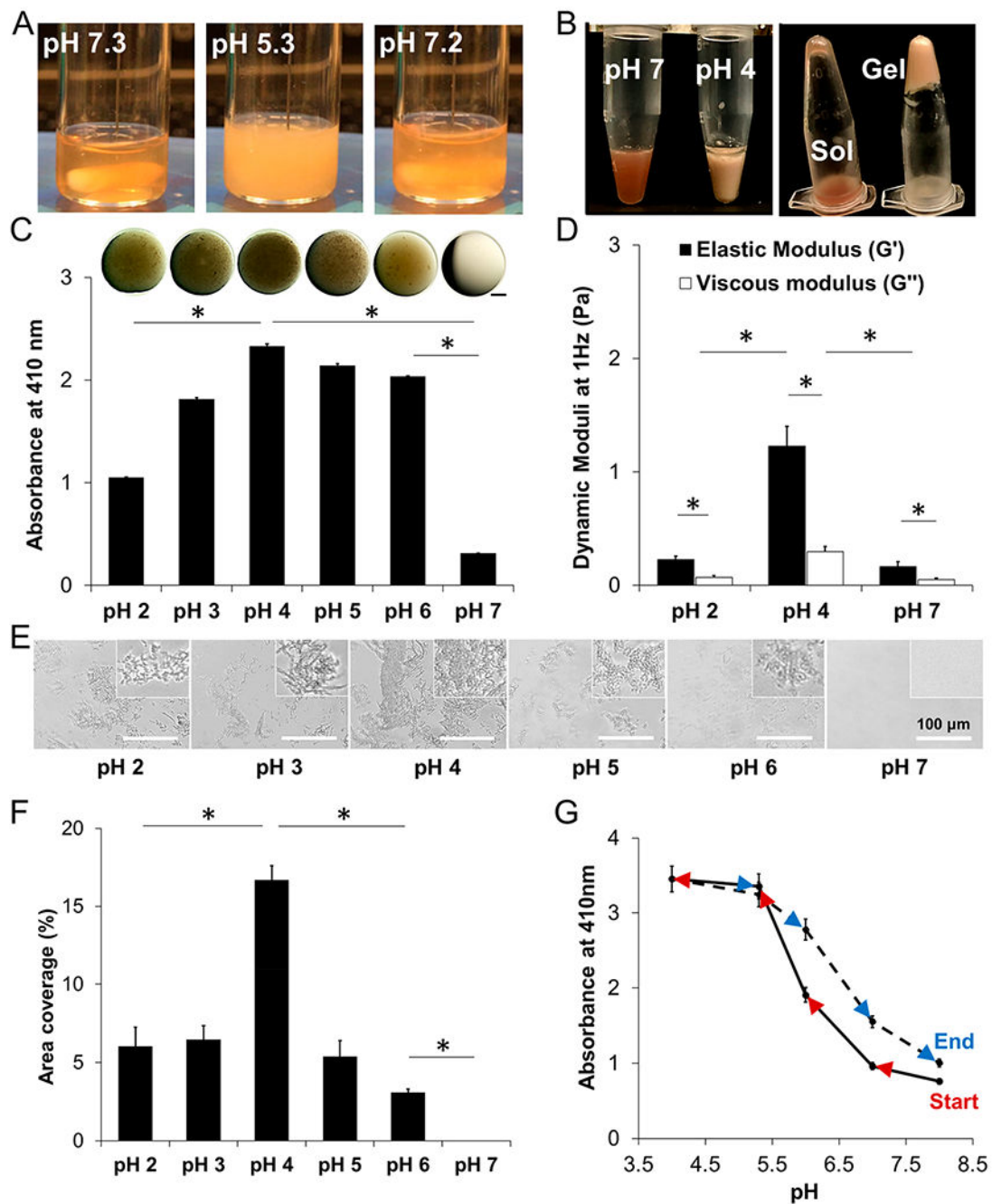


Figure 2.

Response of PSIM to pH. (A) PSIM (20 mg/mL) in 20 mM HEPES at pH 7.3 was clear. At pH 5.3, the PSIM solution was turbid. Returning the pH to 7.2, after decreasing it to 5.3, restored optical clarity. All solutions had a concentration of 20 mg/mL, unless otherwise noted. (B) PSIM (80 mg/mL) in 20 mM HEPES at pH 7 was a viscous solution (left tube, left image) that flowed after inversion (left tube, right image). At pH 4, PSIM was a gel (right tube, left image) that did not flow after inversion (right tube, right image). (C, top) Droplets of PSIM (20 mg/mL) on a glass slide imaged using a stereoscope. Darkness was

due to the turbidity of the droplets. (C, bottom) Absorbance of PSIM solutions (20 mg/mL) at different pH values at a wavelength of 410 nm. (D) Dynamic rheological moduli (G' and G'') of PSIM at pH 2, 4, and 7 and at 1 Hz and 37 °C ($n = 3$, mucus from individual pigs). (E) Microscopic images of PSIM between two glass coverslips in the pH range of 2–7. Insets show close-up images of aggregates. (F) Surface area covered by PSIM aggregates per image (as in panel E) in the pH range 2–7 ($n = 10$). (G) Real-time sampling and characterization of the reversible aggregation of PSIM in the pH range of 4–8. The solid line represents an increase in the absorbance as the pH was reduced from 8 to 4 (red arrows). The dotted line represents the decrease in absorbance (blue arrows) as the pH was increased from 4 to 8 ($n = 3$; *, $P < 0.05$).

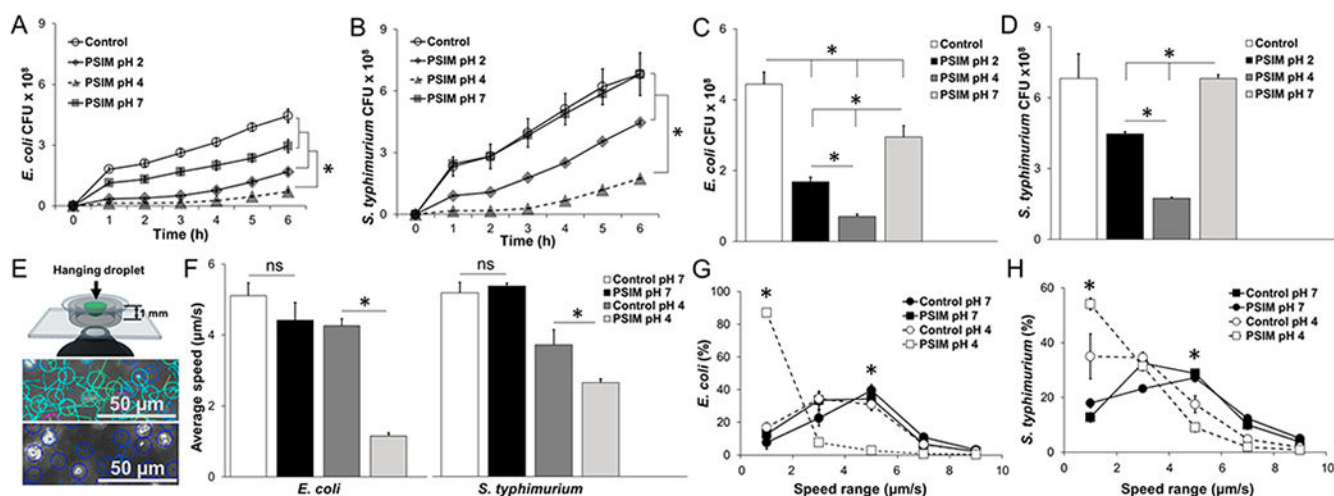


Figure 3. Barrier function of PSIM. (A) Time-resolved transmigration of *E. coli* through 3 μm pore transwell membranes layered with PSIM at pH 7, 4, and 2. Controls were HEPES buffer at pH 7 without PSIM ($n = 3$). (B) Transmigration of *Salmonella*. (C) Number of *E. coli* that migrated across the PSIM layers at a time point of 6 h. (D) Number of *Salmonella* that migrated across the PSIM layers at 6 h. (E) The speeds of individual bacteria were measured in hanging drops of PSIM mixed with bacteria and suspended above the objective of an inverted microscope. At pH 7 (top), velocities (indicated by line lengths) were greater than those observed at pH 4 (bottom), where all bacteria were visibly nonmotile. (F) The average speeds of *E. coli* and *Salmonella* in PSIM at pH 4 were significantly lower than PSIM-free controls at pH 4 (*, $P < 0.05$; $n = 3$). At pH 7, PSIM had no effect on bacterial motility, compared to control. (G) Distribution of speeds of *E. coli* in PSIM at pH 4 and 7, compared to controls (HEPES buffer without PSIM; $n = 3$). The percentage of bacteria with speeds of $< 2 \mu\text{m/s}$ was greater in PSIM at pH 4, compared to pH 7 and controls (*, $P < 0.05$). The percentage of bacteria swimming at $5 \mu\text{m/s}$ was lower in PSIM at pH 4, compared to that observed at pH 7 and for the controls (*, $P < 0.05$). (H) The distribution of speeds of *Salmonella* in PSIM at pH 4 and 7, compared to controls was functionally similar to *E. coli*.

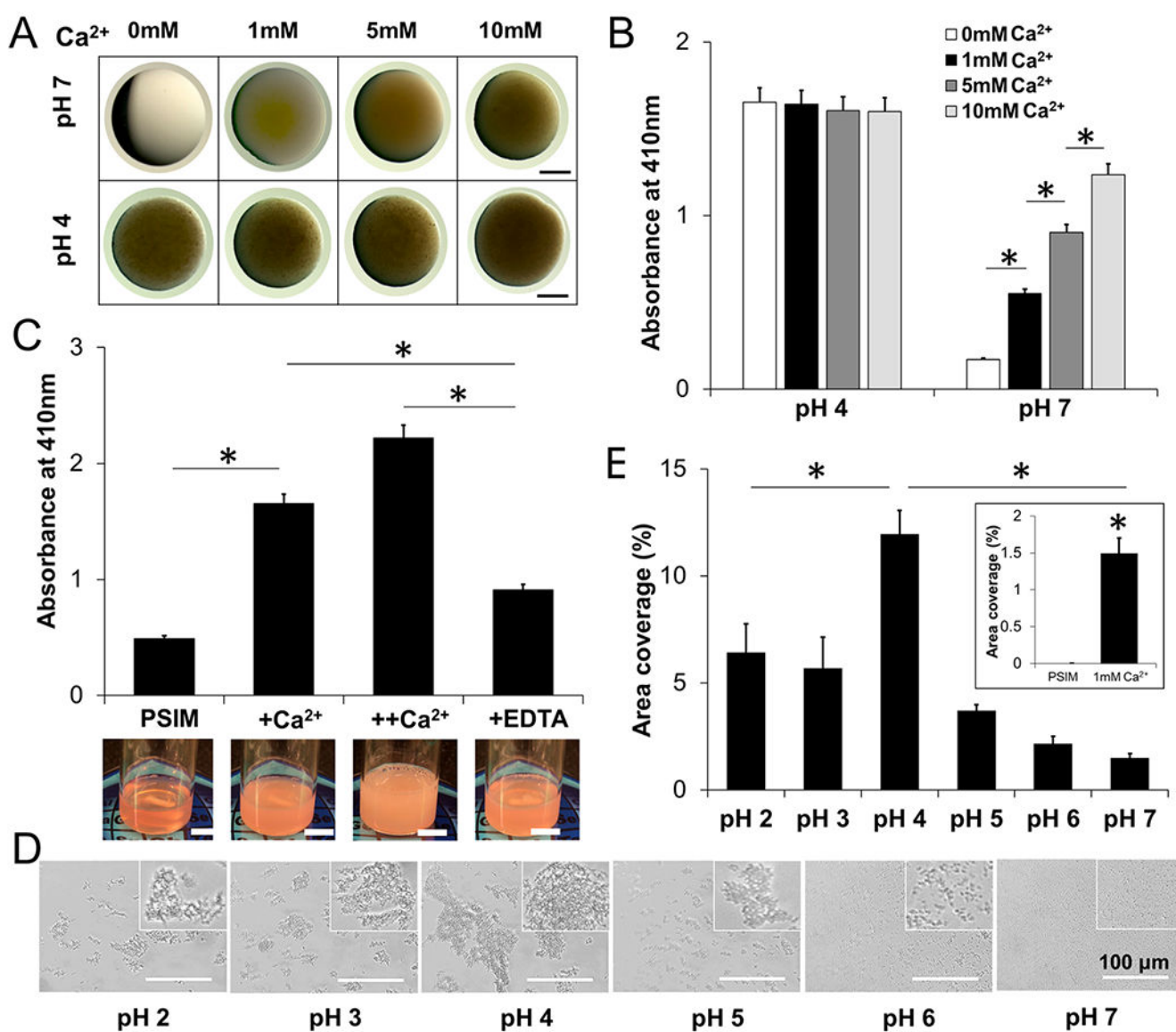


Figure 4.

Calcium regulates the physical properties of PSIM. (A) Stereoscope images of PSIM at pH 4 and 7 with Ca²⁺ ranges from 0 to 10 mM. Scale bar = 1 mm. (B) The absorbance of PSIM at 410 nm and pH 7 increased as the Ca²⁺ concentrations increased to 0, 1, 5, and 10 mM (*, $P < 0.05$; $n = 3$). Absorbance did not change at pH 4. (C) The absorbance of PSIM at 410 nm and pH 7 with 100 μ L of Ca²⁺ (+Ca²⁺) was greater than that of control PSIM without Ca²⁺ (*, $P < 0.05$; $n = 3$). A second addition of 100 μ L Ca²⁺ (++) further increased absorbance. The absorbance was reduced by adding 100 μ L of EDTA (+EDTA), a Ca²⁺ chelator, compared to +Ca²⁺ and ++Ca²⁺ (*, $P < 0.05$). Inset images are snapshots of PSIM solutions at the different Ca²⁺ conditions. Scale bar = 10 mm. (D) Microscopic images of reconstituted PSIM (2% w/v) between two glass coverslips in a pH range of 2–7 with 1 mM Ca²⁺. Insets show close-up images of the aggregates. (E) The surface area covered by PSIM aggregates with 1 mM Ca²⁺ was greatest at pH 4, compared to pH 2–3 and pH 5–6 (*, $P <$

0.05; $n = 10$). At pH 7 (inset), the surface area covered by PSIM aggregates with 1 mM Ca^{2+} was greater than the area covered by PSIM aggregates without Ca^{2+} (*, $P < 0.05$).

Author Manuscript

Author Manuscript

Author Manuscript

Author Manuscript

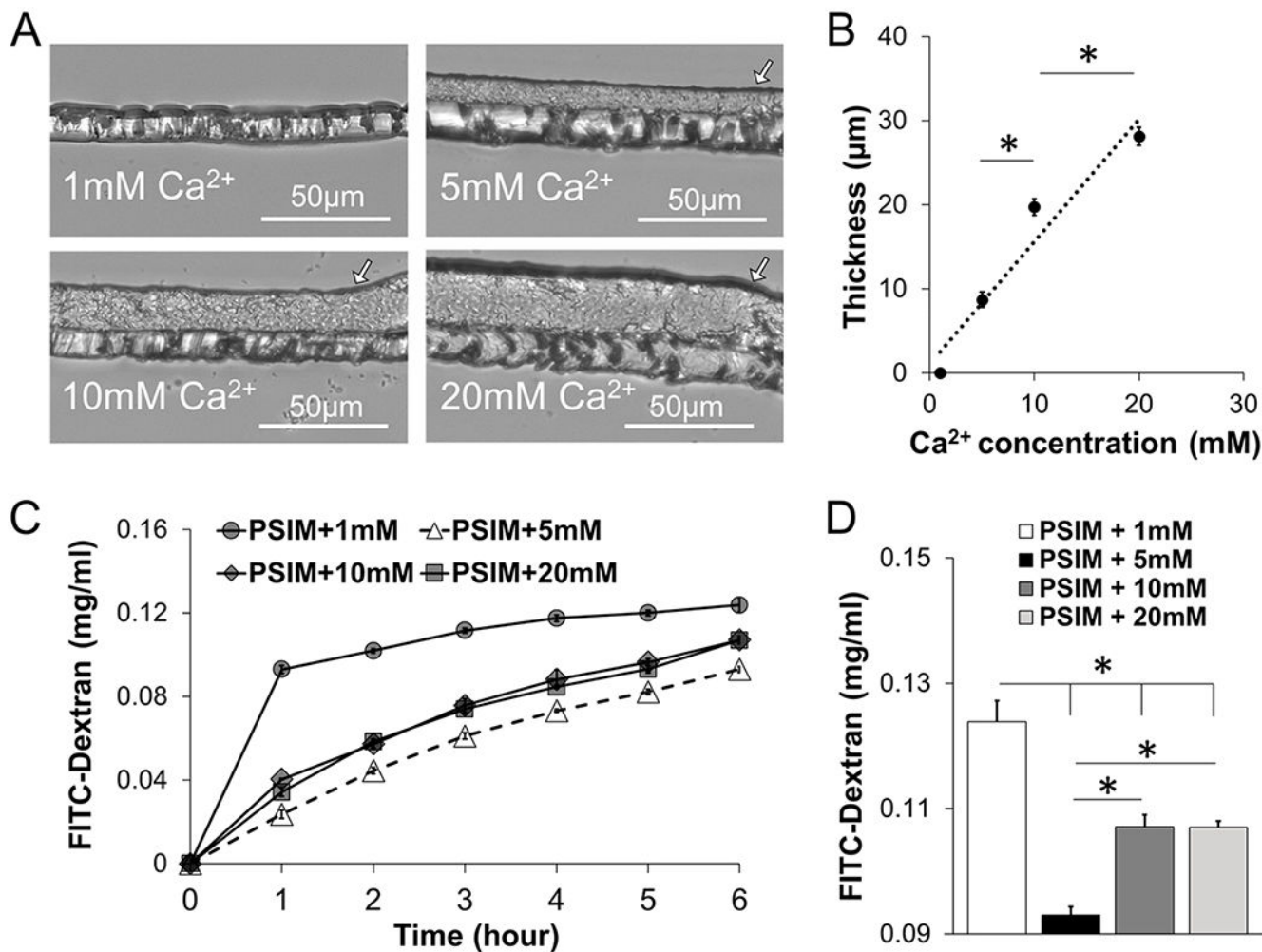


Figure 5. Calcium controls the thickness of the mucus barrier. (A) Cross-section images of PSIM gel layers formed on transwell membranes at 1, 5, 10, and 20 mM Ca²⁺ and pH 7. (B) PSIM layer thickness increased linearly with Ca²⁺ concentration. The thicknesses at 10 and 20 mM were greater than those observed at 5 and 10 mM, respectively (*, $P < 0.05$; $n = 3$). (C) Concentration of FITC-dextran after transport through a PSIM layer formed on a transwell membrane in the presence of 1, 5, 10, and 20 mM Ca²⁺ at pH 7. (D) Concentration of FITC-dextran at 6 h after transport through the PSIM layers in panel (C). The concentration was greatest with 1 mM Ca²⁺, compared to all other concentrations (*, $P < 0.05$; $n = 5$). The concentration of FITC-dextran was less at 5 mM, compared to that observed at 10 and 20 mM Ca²⁺.

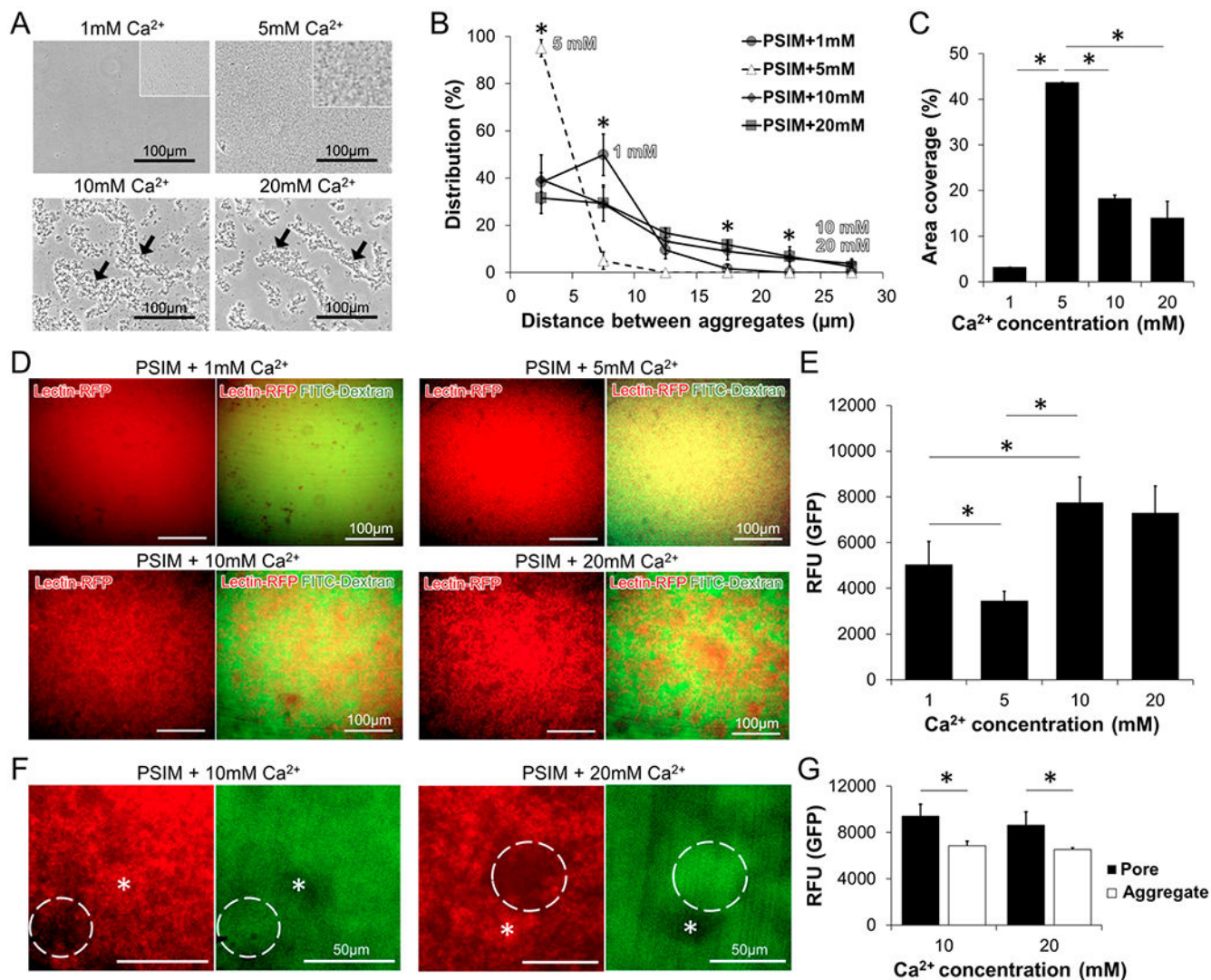


Figure 6. Calcium controls the porosity of the mucus barrier. (A) Microscopic images of PSIM aggregates at 1, 5, 10, and 20 mM Ca^{2+} and pH 7. Higher resolution images show homogeneous, dense, and small PSIM aggregates at 5 mM Ca^{2+} . (B) Distribution of distances between PSIM aggregates, as a function of Ca^{2+} concentration. The percentage of distances $< 5 \mu\text{m}$ was greater at 5 mM, compared to those observed at 1, 10, and 20 mM (*, $P < 0.05$; $n = 5$). The percentage of distances between 5 and 10 μm was greater at 1 mM, compared to that observed at 5 mM (*, $P < 0.05$). The percentage of distances between 15 μm and 25 μm was greater at 10 and 20 mM, compared to that observed at 1 and 5 mM (*, $P < 0.05$). (C) The surface area covered by the PSIM-aggregates at 5 mM was greater than that observed at both 1 and 10 mM Ca^{2+} (*, $P < 0.05$; $n = 10$). (D) Fluorescent microscopic images of Cy5-lectin-tagged PSIM layers (red, left) and overlaid with FITC-dextran (green, right) at 1, 5, 10, and 20 mM Ca^{2+} . (E) The average GFP fluorescence (in relative fluorescence units, RFU) was less at 5 mM, compared to that observed at 1, 10, and 20 mM (*, $P < 0.05$; $n = 5$). (F) Expanded images of pores (dashed lines) and aggregates (stars)

formed in PSIM layers at 10 and 20 mM Ca^{2+} . (G) The fluorescence intensity of FITC-dextran in pores was greater than that observed in aggregates at both 10 and 20 mM Ca^{2+} (*, $P < 0.05$; $n = 5$).

Author Manuscript

Author Manuscript

Author Manuscript

Author Manuscript

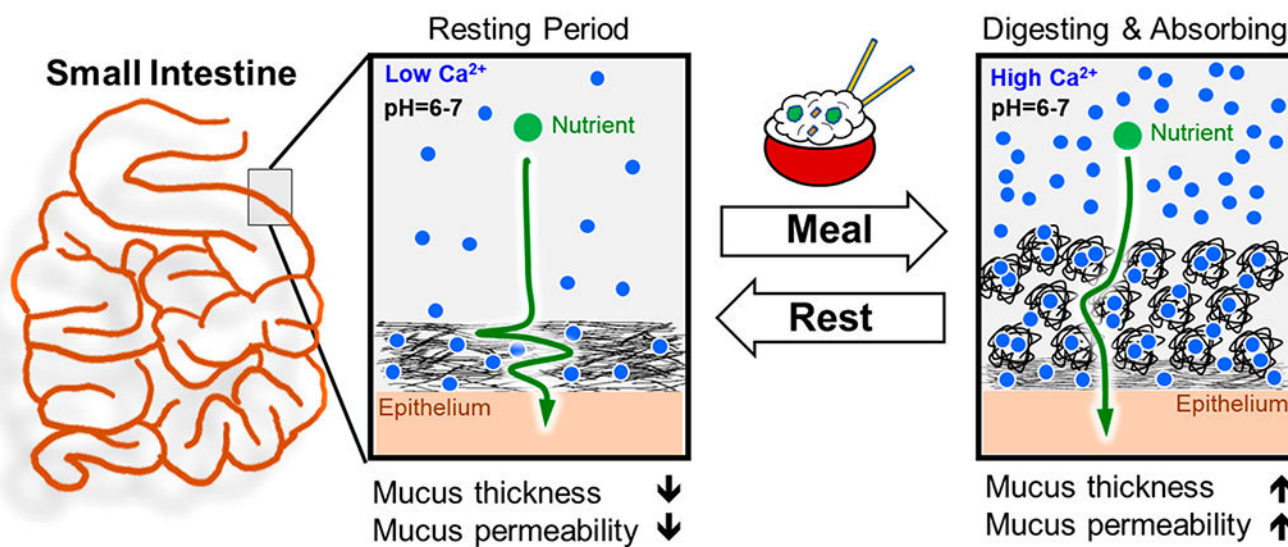


Figure 7. Role of calcium as a regulator of molecular transport. Proposed dynamic regulation of the thickness and permeability of the small intestine mucus barrier in response to available luminal Ca^{2+} ions that fluctuate between meals.